Received: 2 January 2023 | Accepted: 21 May 2023

DOI: 10.1002/nsg.12260

Near Surface Geophysics EAGE EUROPEAN ASSOCIATION OF GEOSCIENTISTS & ENGINEERS

ORIGINAL ARTICLE

# Soil resistivity measurements to evaluate subsoil salinity in rice production systems in the Vietnam Mekong Delta

**Van Hong Nguyen**[1] | **Jörn Germer**[1] | **Van Nha Duong**[2] | **Folkard Asch**[1]

[1]Institute of Agricultural Sciences in the Tropics (Hans-Ruthenberg Institute), University of Hohenheim, Stuttgart, Germany

[2]Agriculture and Rural Development Faculty, Kien Giang University, Châu Thành, Kiên Giang, Vietnam

**Correspondence**
Folkard Asch, Institute of Agricultural Sciences in the Tropics (Hans-Ruthenberg Institute), University of Hohenheim, Stuttgart, Germany.
Email: fa@uni-hohenheim.de

**Funding information**
Bundesministerium für Bildung und Forschung; Federal Ministry of Education and Research (BMBF, Germany), Grant/Award Number: 031B0724

## Abstract

Rice is a staple crop in the Vietnam Mekong Delta (VMD) in which more than half of Vietnam's rice is produced. However, rice production in the VMD is threatened by increasing saltwater intrusion due to land subsidence and climate change induced sea level rise. Saltwater intrusion into lowland areas through the canal system or capillary rise of saline water from near surface saline water tables may result in salt accumulation in the topsoil. Therefore, it is important to disentangle the two effects and their relative importance to implement appropriate strategies for water and salinity management for adapting rice production systems of the VMD to climate change. Here, we report on the possibility of using geoelectrical methods to evaluate the potential threat of subsoil salinity to rice production. To evaluate the level of subsoil salinity, we measured soil electrical resistivity using an ARES II to a depth of 40 m in a case study comprising five locations in the VMD. Electrical resistivity measurements were calibrated to soil types, which were identified through evaluating 1 m core sections obtained by drilling down to 40 m depth. The relationship between drilling data and soil resistivity was determined by applying clustering and principal component analysis. Resistivity values smaller than 3 Ω m were clearly identified as indicative for a saline water table. The results show a direct link between the depth of the saline water table and the proximity to the sea, but not to the rice production system (single, double, or triple cropping). This study proved for the first time the applicability of the electrical resistivity tomography method for identifying groundwater tables and evaluating subsoil salinity on an agricultural field scale in the VMD.

**KEYWORDS**
conductivity, electrical resistivity tomography, groundwater, site effect

## INTRODUCTION

The Vietnam Mekong Delta (VMD) is an alluvial delta that covers approximately 39,000 km$^2$ comprising an irrigation canal system of about 10,000 km length (Van Kien et al., 2020). Rice production, aquaculture of shrimps and fish, as well as fruit production, are the main agricultural activities contributing 50%, 65% and 70% of Vietnam's total production, respectively. Depending on water quality and availability, rice is produced as single, double, or triple crop annually on the same area. Rice production in the VMD contributes 90% of Vietnam's rice exports (Schneider & Asch, 2020).

The fresh water supply for agricultural production in the low-lying delta with an average elevation of less than 1 m above mean sea level (Minderhoud et al., 2019) is threatened by saltwater intrusion caused by land subsidence and climate change induced sea level rise. Saltwater intrusion is aggravated by an increasing number of dams in the upstream of the Mekong River leading to reduced discharge flows (CGIAR, 2016). Triggered by an extreme drought, the saltwater

intrusion in 2016 caused a freshwater shortage that affected 339,000 ha of rice production (Yen et al., 2019) and caused severe yield losses during the winter/spring rice crop (FAO, 2016). Saltwater also intrudes into the near surface groundwater layers that are directly recharged from surface water (Nguyen et al., 2021; Tran et al., 2022).

Various approaches have been proposed for the VMD to cope with seasonally limited freshwater availability, such as changing cropping patterns or using water-efficient irrigation techniques. However, as irrigation practices, such as alternative wetting and drying irrigation, increase capillary rise from shallow water tables (Tan et al., 2014), salt may intrude into the top soil if the shallow groundwater is saline.

Geoelectric surveying is a non-invasive and cost-effective method for exploring the structure of the earth's subsurface and is used, for example, in groundwater exploration, monitoring landfills or agronomical management (Samouëlian et al., 2005). Common applications of geoelectric surveys are to detect and map groundwater (Mohamaden & Ehab, 2017; Riwayat et al., 2018), identify specific subsurface features, such as gypsum deposits (Gołębiowski & Jarosińska, 2019), and investigate saltwater intrusion into coastal areas and alluvial deltas (Cong-Thi et al., 2021; de Franco et al., 2009; Gemail et al., 2004; Galazoulas et al., 2015; Nowroozi et al., 1999).

In agricultural research, electrical resistivity tomography (ERT) is increasingly being used for monitoring soil moisture content (Rao et al., 2020), evaluating the effectiveness of irrigation systems on field scale through the spatio-temporal variation of soil moisture content (Araya et al., 2021), and, as recently reviewed by Cimpoiaşu et al. (2020), the relationship between resistivity and water uptake by plants under different irrigation conditions.

The aim of this study was to identify near surface water tables and assess their salinity at five case study sites contrasting in land use (single, double, and triple rice cropping) and proximity to the sea using ERT at agricultural field scale and to evaluate potential risks for capillary rise of saline ground water.

## MATERIALS AND METHODS

### Research area

Near surface water tables were identified at five sites with contrasting land-use in Tra Vinh province, a coastal province in the eastern VMD (Figure 1). The province lies between two main arms of the Mekong River and is pervaded by a system of irrigation and drainage canals. Under tidal influence, deposition of mud, silt, sand and gravel at the mouths of the Mekong's distributaries formed a floodplain of lowland swamps and sand dunes as typical topographic patterns. The elevation of the Tra Vinh province varies from 1 m to 3 m above mean sea level (Tran, 2020).

### Resistivity measurements

During a dry season in the case study in the VMD, soil electrical resistivity was measured using ARES II (GF Instruments s.r.o., Czech Republic). The ARES II/1 control unit was used with six 1-channel multi-electrode cables (eight electrodes per cable) connecting the stainless-steel electrodes and inserted into the ground. The electrodes were arranged following the Wenner–Schlumberger array configuration (Loke, 2021) along the bunds of the fields to allow measuring also when fields were flooded. Electrode spacings of 2, 3, 4 and 5 m allowed for effective measuring depths of 20–50 m. The roll-along technique was applied to extend the measurement line by moving the first cable to the end of the line to continue the measurement (Loke, 2021). At site S5, only one profile with 4 m electrode spacing was measured as the shrimp farm did not have parallel bunds of the same length. The number of electrodes used was a function of profile length and electrode spacing at the respective sites (Table 1). The 4 m electrode spacing was used in the analysis and for calibration with drilling data (see, section '2D ERT profiles').

For three-dimensional (3D) mapping of resistivity, depending on site layout, five, three, six and eight parallel ERT profiles were measured at S1–S4, respectively.

ARES II measurements were processed with RES2DInv (version 4.10.8) to invert separate two-dimensional (2D) resistivity profiles and RES3DInv (version 3.18.4) to generate 3D resistivity maps from 2D parallel ERT profiles. The processing programmes use the smoothness-constrained Gauss–Newton least-squares method to produce a 2D or 3D model of the subsurface (Loke, 2021). The resistivity obtained from inversion procedure was visualized as contour graphs by using Surfer software (Golden Software, LLC).

### Boreholes drilling

Boreholes were drilled by applying the rotary wash boring method using the drilling machine XY-1 (Zhengzhou Defy Mechanical & Electrical Equipment Co., Ltd.). During the drilling process, soil samples were collected from each 1 m down to 40 m depth of the boreholes. Soils from the cores were taken as undisturbed samples using a thin wall tube with $\Phi = 75$ mm. Soil samples were separated in two parts: (1) stored in sealed and labelled plastic tubes ($\Phi = 75$ mm, 20 cm in length) as undisturbed samples to analyse soil properties at the

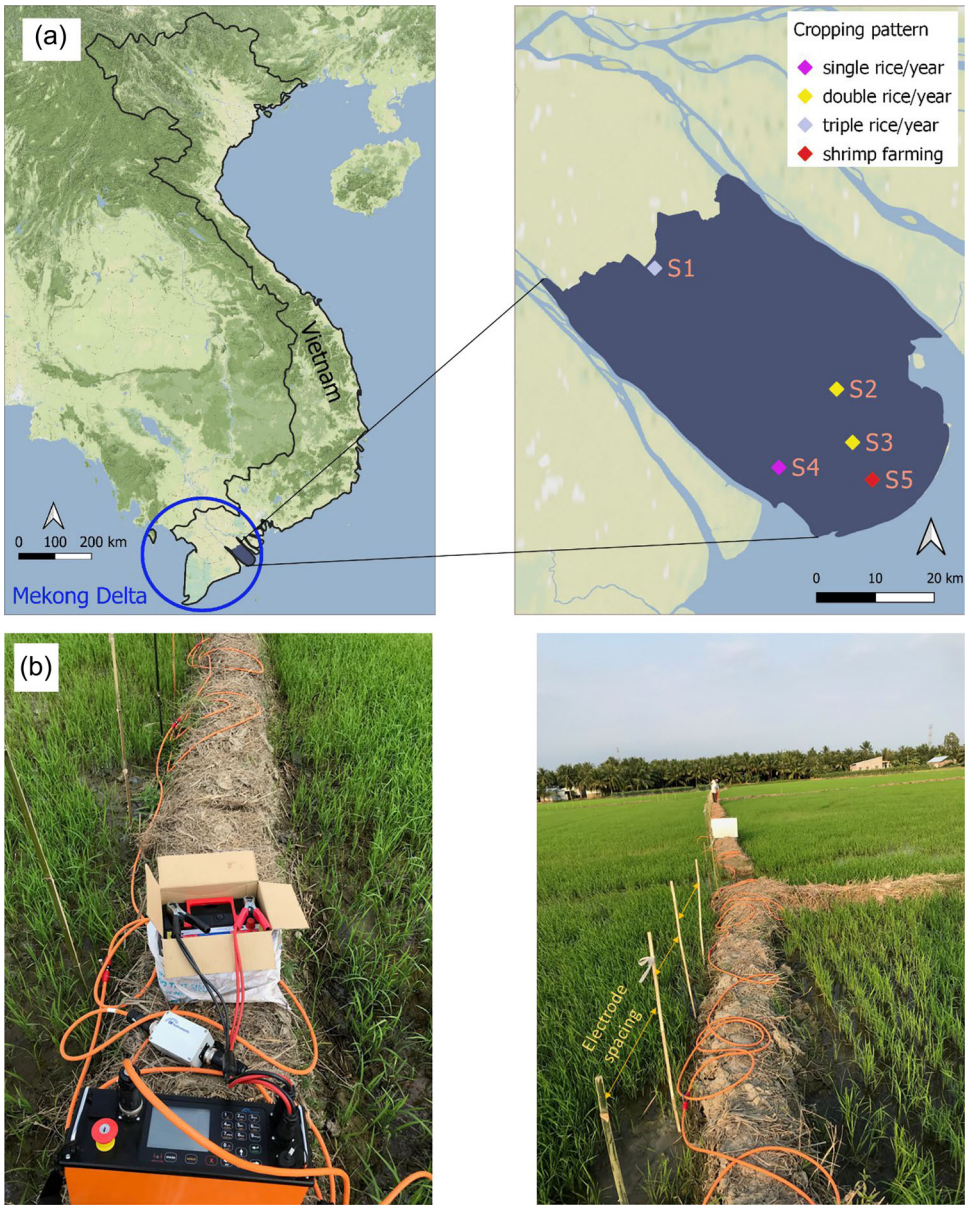


**FIGURE 1** Location of the study area and in situ measurement of soil resistivity. (a) Map of the case study area in the Vietnam Mekong Delta including the five contrasting study sites. The sites represent different land-use types: S1 = triple rice cropping, S2, S3 = double rice cropping, S4 = single rice cropping – no shrimp production and S5 = shrimp production. (b) ARES II measurement in the field with electrode spacing marked with bamboo sticks.

laboratory and (2) stored in labelled plastic bags to test electrical conductivity (EC) of the soil.

EC of the soil was measured using a Portable Multi-range Conductivity Meter (HI-8733, Hanna Instruments Ltd.), from 100 g soil suspended in water at a soil–water ratio of 1:5 at the end of each drilling day. From the undisturbed core samples moisture content, density, porosity, degree of saturation and soil structure was determined by the Laboratory of Soil Mechanics Construction Materials (Ho Chi Minh City, Vietnam).

In addition, during the drilling process, the drainage water from each sample core was collected for EC measurement with the mentioned conductivity meter.

## Statistical analyses

Statistical analyses were performed with R (v4.1.14; R Core Team, 2021). The relationship between the resistivity of the soil sampled from the borehole cores, the soil properties and the presence of saltwater was analysed using heat map (pheatmap package (v1.0.12; Kolde, 2019)). Heat map clustering with hierarchical analysis was applied to detect patterns and similarities in the data set. A principal component analysis (PCA) was performed subsequently to confirm the clusters extracted from the heat map to find factors that influence soil resistivity. Eight variables were selected for

**TABLE 1** Site-specific profile lengths, number of electrodes (number in parentheses) used with different electrode spacings, water table level, maximum and minimum electrical conductivity of water and soil in the drill cores and soil resistivity extracted from the electrical resistivity tomography (ERT) profile at the borehole location corresponding to 2, 3, 4 and 5 m electrode spacing.

| Site | | | S1 | S2 | S3 | S4 | S5 |
|---|---|---|---|---|---|---|---|
| Profile length (m) and [number of electrodes] | | 2 m | 318 [160] | 190 [96] | 190 [96] | 190 [96] | – |
| | | 3 m | 333 [112] | 189 [64] | 189 [64] | 189 [64] | – |
| | | 4 m | 348 [88] | 188 [48] | 188 [48] | 188 [48] | 252 [64] |
| | | 5 m | 315 [64] | – | – | – | – |
| Water table (m) | | | 8 | 5 | 4 | 4 | 3 |
| EC_water (mS $cm^{-1}$) | | Max | 6.1 | 5.7 | 6.0 | 7.9 | 49.6 |
| | | Min | 2.0 | 3.0 | 3.7 | 4.8 | 31.6 |
| EC_soil (mS $cm^{-1}$) | | Max | 2.7 | 2.1 | 2.2 | 3.4 | 4.6 |
| | | Min | 1.2 | 1.0 | 1.0 | 1.2 | 2.1 |
| Resistivity (Ω m) | 2 m | Max | 16.2 | 386.1 | 160.4 | 27.5 | – |
| | | Min | 1.5 | 0.7 | 0.6 | 0.6 | – |
| | 3 m | Max | 19.5 | 74.8 | 83.0 | 18.9 | – |
| | | Min | 1.2 | 1.1 | 0.6 | 0.6 | – |
| | 4 m | Max | 12.3 | 61.9 | 147.2 | 11.2 | 3.2 |
| | | Min | 1.1 | 1.2 | 0.4 | 0.6 | 0.3 |
| | 5 m | Max | 8.0 | – | – | – | – |
| | | Min | 1.1 | – | – | – | – |

cluster analysis, namely sand, clay, moisture content, bulk density, cropping types, EC of water and soil and resistivity.

## RESULTS AND DISCUSSION

### 2D ERT profiles

Figure 2 shows the ERT profiles of site S1–S4 at the location of the boreholes measured with varying distances between the electrodes of the ARES II. Low resistivity (<2 Ω m) values indicate the presence of water. Measurements with a distance of 2 m between the electrodes allow a penetration depth of up to 20 m. At sites S1 and S4, the 2 m electrode spacing did not cover the depth necessary to assess the entire dimension of the low resistivity zone as the resistivity values stayed low up to 20 m depth. Similarly, a 3 m spacing indicated the end of the low resistivity zone at about 25 m depth at site S4, whereas no boundary was evident at site S1. At a 4 m spacing, the upper and lower limits of the low resistivity zone were evident at all sites. The maximum depth of the low resistivity zone at about 40 m at site S1 was confirmed by measuring a profile with 5 m spacing between the electrodes (data not shown). As the paddy fields in the Mekong delta are relatively small and the minimum length of bunds needed for 5 m spacing of electrodes is about 240 m, measuring at 5 m spacing was only possible at site S1. Therefore, we conclude that ERT using 4 m electrode spacing to be most suitable for assessing soil resistivity at sufficient depth in the paddy fields of the study area.

In general, the highest resistivity (>20 Ω m) was found at the surface of each site, whereas the lowest resistivity (<3 Ω m) was measured at medium depths (10–20 m) of all ERT profiles and all sites.

Based on the resistivity ranges from the ERT profiles and the location of the sites, three different resistivity zones were distinguished. S4, located near the sea and representing a single rice crop/year, was in the zone with the lowest resistivity (0.2–15.0 Ω m). Sites S3 and S2 were grouped into the high resistivity zone (0.8–184.2 Ω m) and S1, northern most site of the study area, in the medium resistivity zone (1.24–12.00 Ω m). The maximum and minimum resistivities of the ERT profiles at the five sites are summarized in Table 1.

### 3D resistivity maps

Multiple profiles were used to generate 3D resistivity maps for the four case study sites shown in Figure 3, which were measured with an electrode spacing of 4 m. The 3D soil resistivity maps are similar to the 2D ERT profiles in terms of low resistivity at the medium depths. However, the resolution of the interpolated 3D maps in the upper and lower soil depths is lower than in the original 2D maps, and at these depths, the layers of higher electrical resistivity are located. Lowest resistivity was measured below 6 m depth at site S1 and from 8 to 20,

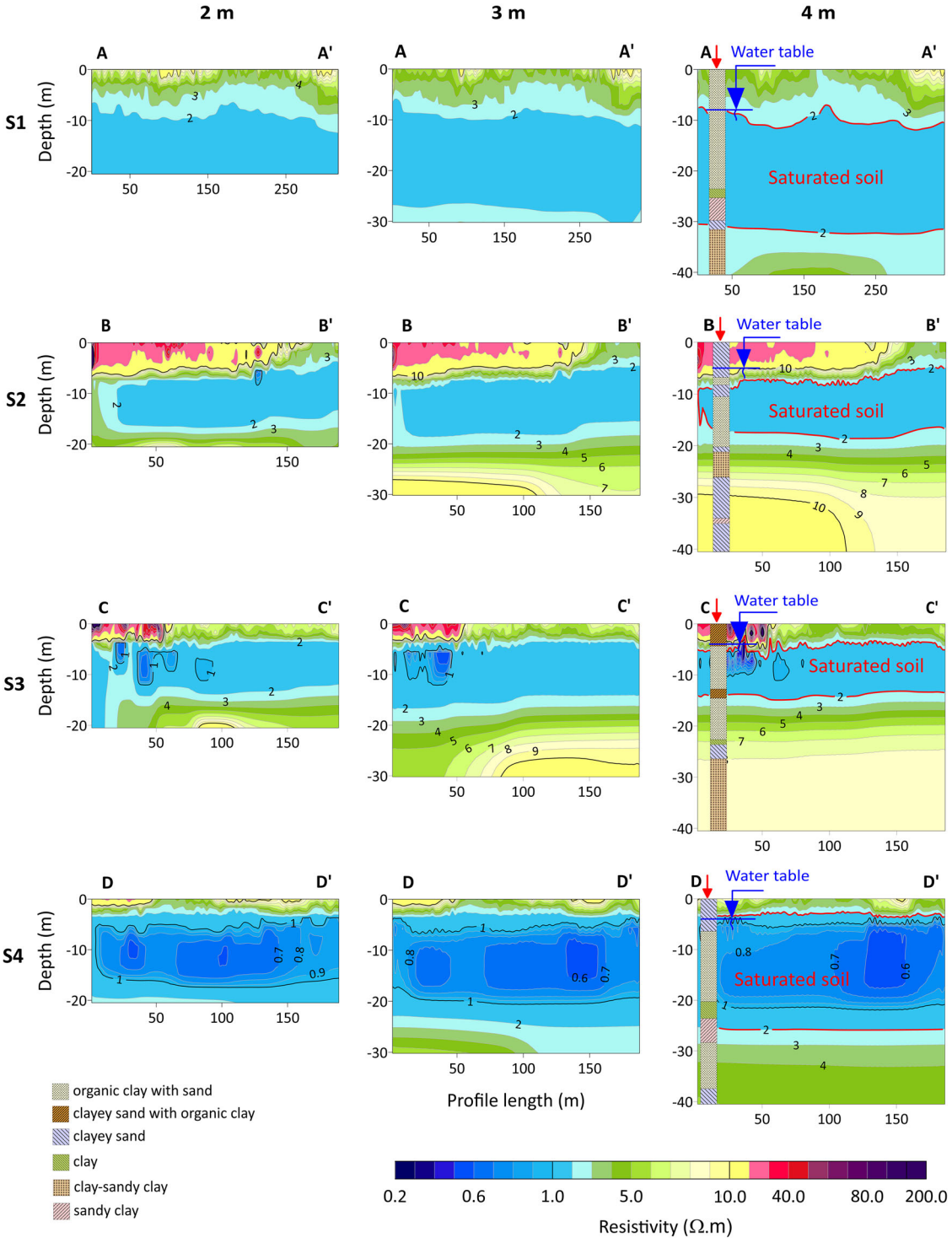


**FIGURE 2** Two-dimensional (2D) electrical resistivity profiles with electrode spacing = 2 m, 3 m and 4 m at the four sites: S1 – triple rice/year, S2, S3 – double rice/year and S4 – single rice/year. The length of profiles depends on the size and bunds in each rice paddy, site S1 having the longest straight bunds. The contour interval is 1 Ω m. The colours of electrical resistivity tomography (ERT) profiles are displayed in logarithmic scale. The letters A–A′, B–B′, C–C′ and D–D′ represent for sections marked in Figure 3. The arrows indicate the position of the boreholes. Soil properties of the boreholes are stacked in ERT profiles as borehole logs.

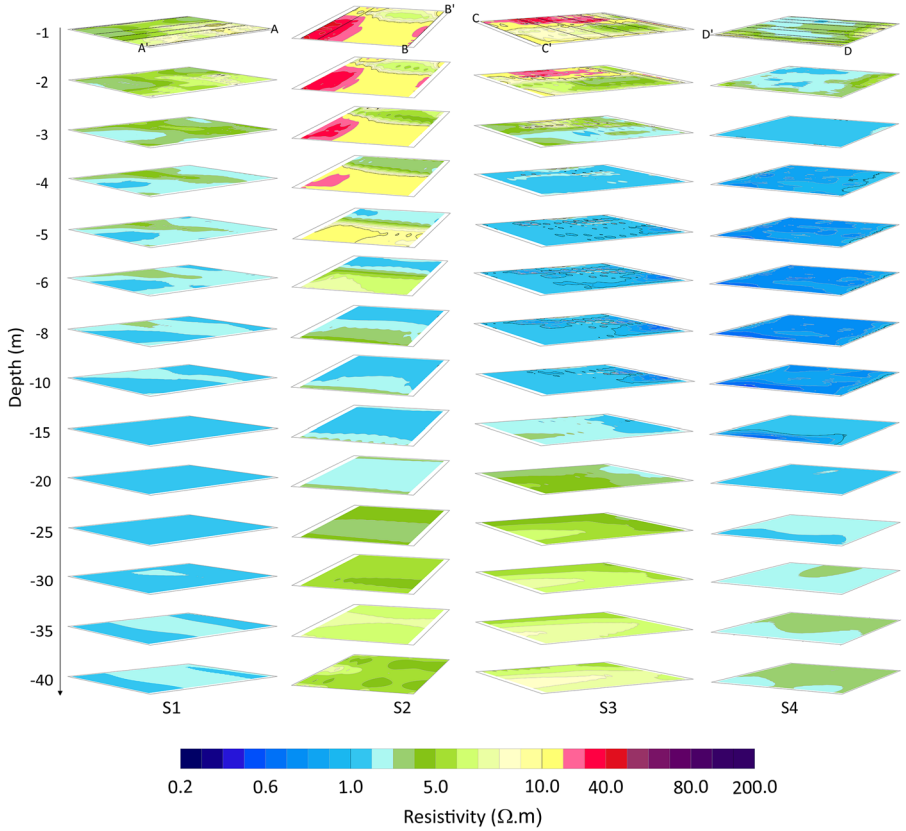


**FIGURE 3** Three-dimensional (3D) resistivity maps obtained with 4 m electrode spacing for the four case study sites in true north orientation. From 1 to 6 m depth, the 3D planes are displayed at 1 m intervals due to high variation of resistivity in the upper soil layers. The intervals increase from 2 to 5 m for depths from 6 to 10 m and from 10 to 40 m depth, respectively, related to the homogeneity of soil properties and the decrease in electrical resistivity tomography (ERT) profile resolution. The colours represent resistivity on a logarithmic scale. Dotted lines on the surface layer at each site indicate the sections where two-dimensional (2D) ERTs were measured. The cross sections illustrated by A–A′, B–B′, C–C′ and D–D′ are the 2D ERT lines coinciding with borehole positions.

4 to 15 and 3 to 30 m at site S2, S3 and S4, respectively. The layer of low resistivity (<3 Ω m) approaches the surface as the distance to the sea decreases. As confirmed by the drilling data in Table 1, resistivity below 10 Ω m (yellow colour in Figure 3) indicates water saturated soil.

## Calibrating electrical resistivity against soil properties

Site-specific electrical resistivity is known to be strongly influenced by soil properties, such as soil structure, moisture content, or porosity (Samouëlian et al., 2005). Therefore, to calibrate and interpret the resistivity data obtained with ARES II, boreholes were drilled to a depth of 40 m at each site, and the changes in soil and water properties were evaluated for each meter of depth. The data show that the depth of the shallow water table decreases towards the sea, from 8 m depth at site S1 to 3 m depth at site S5. In contrast to all other sites, site S5 shows a significantly higher water EC (>30 mS $cm^{-1}$, Table 1) combined with a low electrical resistivity of the soil (<3 Ω m, Table 1), which, with EC values above 4.5 mS $cm^{-1}$, indicates salinity, according to Brouwer et al. (1985).

Figure 4 illustrates the relationship between EC measurements from the core samples for soil and water and the ERT resistivity values extracted from the ARES II measurements. ERT resistivity of water saturated soil decreased towards the sea, from about 15 Ω m at site S2 to less than 2 Ω m at S5 (Figure 4). Soil layers with high EC water values (EC > 4.5 mS $cm^{-1}$) have ERT resistivity values smaller than 9 Ω m. Site S1 is an exception with low ERT resistivity values (<2 Ω m), where EC values of water do not allow to distinguish freshwater from saltwater, which may be due to differences in soil properties. With ERT resistivity values higher than 3 Ω m, it is clear that the EC of soil and water increases as ERT resistivity decreases, whereas this pattern cannot be seen with ERT resistivity lower than 3 Ω m.

Water tables may not easily be detected due to spatial changes in soil properties that may overlay soil–water boundaries (Palacky, 1987). Equally, high clay contents and, thus, lower resistivity values could be confused with soil salinity or soil moisture (Galazoulas et al., 2015; Giao et al., 2003; Samouëlian et al., 2005; Zohdy et al.,

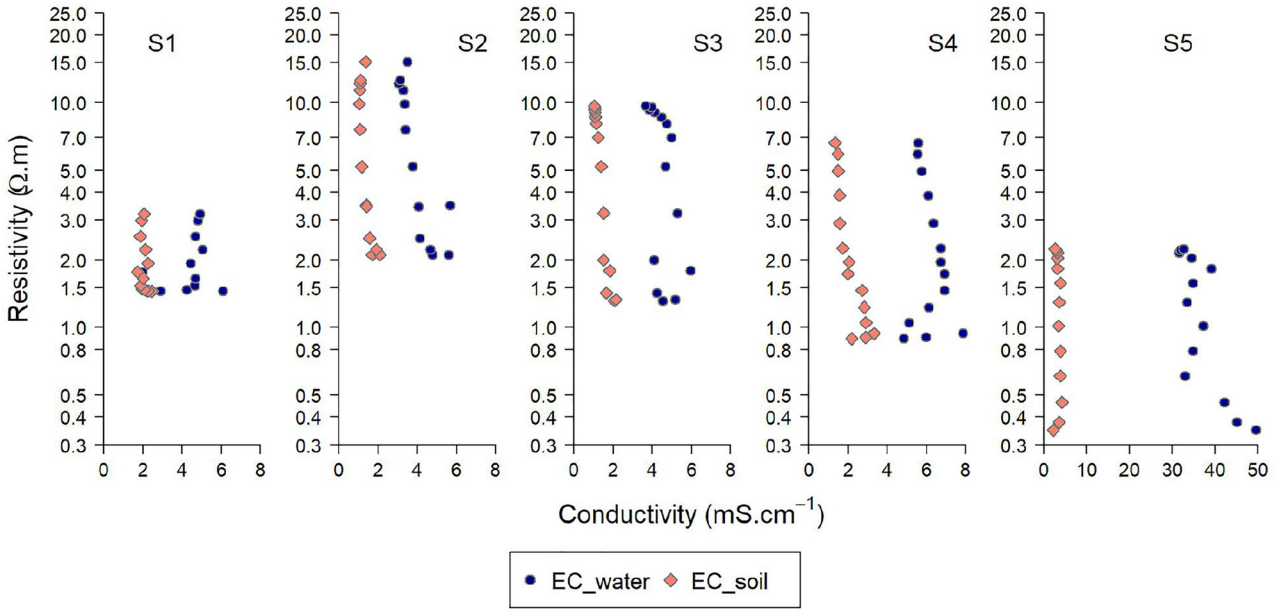


**FIGURE 4** Relationship between electrical conductivity (EC) of soil and water for each 1 m depth interval in the soil core and electrical resistivity tomography (ERT) electrical resistivity values extracted from the ARES II measurement. The *y*-axis is logarithmically scaled.

1993). Figure 5 illustrates the properties of the soil cores drilled at each study site and the respective soil and water EC values as well as electrical resistivity measured. At site S1, EC values of the drainage water from the cores clearly indicate saline water below 20 m depth. However, low resistivity (<2 Ω m) was measured from 10 m to 30 m depth. This shallow layer of low resistivity (10–20 m depth) at S1 was probably due to soil properties such as fine grain size, high porosity and high moisture content (Figure 5a, S1). Although some influence of soil properties on soil resistivity can also be seen at site S2–S4, the sharp decrease of resistivity values at 3–8 m in combination with high EC values clearly indicates the saline water table. The increase of resistivity in greater depths on the other hand may be related to changes in soil structure and moisture content.

## Characteristics of the shallow water table

Based on the range of resistivity of saline water (<4.5 Ω m) (Nowroozi et al., 1999), the low resistivity indicates saline water in the depth from 10 m to 20 m at all case studies sites. This confirms the presence of saltwater in the shallow aquifer in the Mekong delta as previously reported by Ha et al. (2022).

## Relationship between resistivity and soil properties

### Cluster analysis

In Figure 6, the properties of the 1 m borehole core samples are hierarchically analysed in an intensity heat map. The hierarchical analysis groups samples with similar characteristics of the five study sites using the Euclidean distance and complete linkage clustering method (El-Hamdouchi & Willett, 1989; Murtagh & Contreras, 2012). The height of the branches in the dendrogram represents the degree of dissimilarity between clusters; thus, the longer the branch, the greater the differences between clusters (Takahashi et al., 2019). Accordingly, the heat map distinguishes three major groups; A, B and C. Considering detail characteristics at a lower hierarchical level, group C is subdivided into C1 and C2.

Group A clusters samples characterized by high water conductivity larger than 31.6 mS cm$^{-1}$, that is very close to the EC of seawater (Tyler et al., 2017). All these samples belong to S5, which is characterized by its proximity to the sea and its distinct land use pattern (Figures 6 and 7).

Group B is dominated by soils with high proportions of fine grain (>54%) and high moisture content (>43%) (Figures 6 and 7). Resistivity values of the samples clustered in group B are in the narrow range from 0.9 Ω m to 5.9 Ω m, which is the typical range for clay soil (Giao et al., 2003; Shevnin et al., 2006).

Group C clusters samples having low EC values of soil and water (Figures 6 and 7) and predominantly high resistivity. The high resistivity values in this group are mainly due to low soil moisture (<40%). With the exception of S2, it has an exceptionally high resistivity (>5.8 Ω m) due to its high sand content (>75%, Figure 6) and thus forms sub-cluster C1. Sub-cluster C2, on the other hand, represents a sample group with lower resistivity associated with high clay content and high EC of water and soil (Samouëlian et al., 2005).

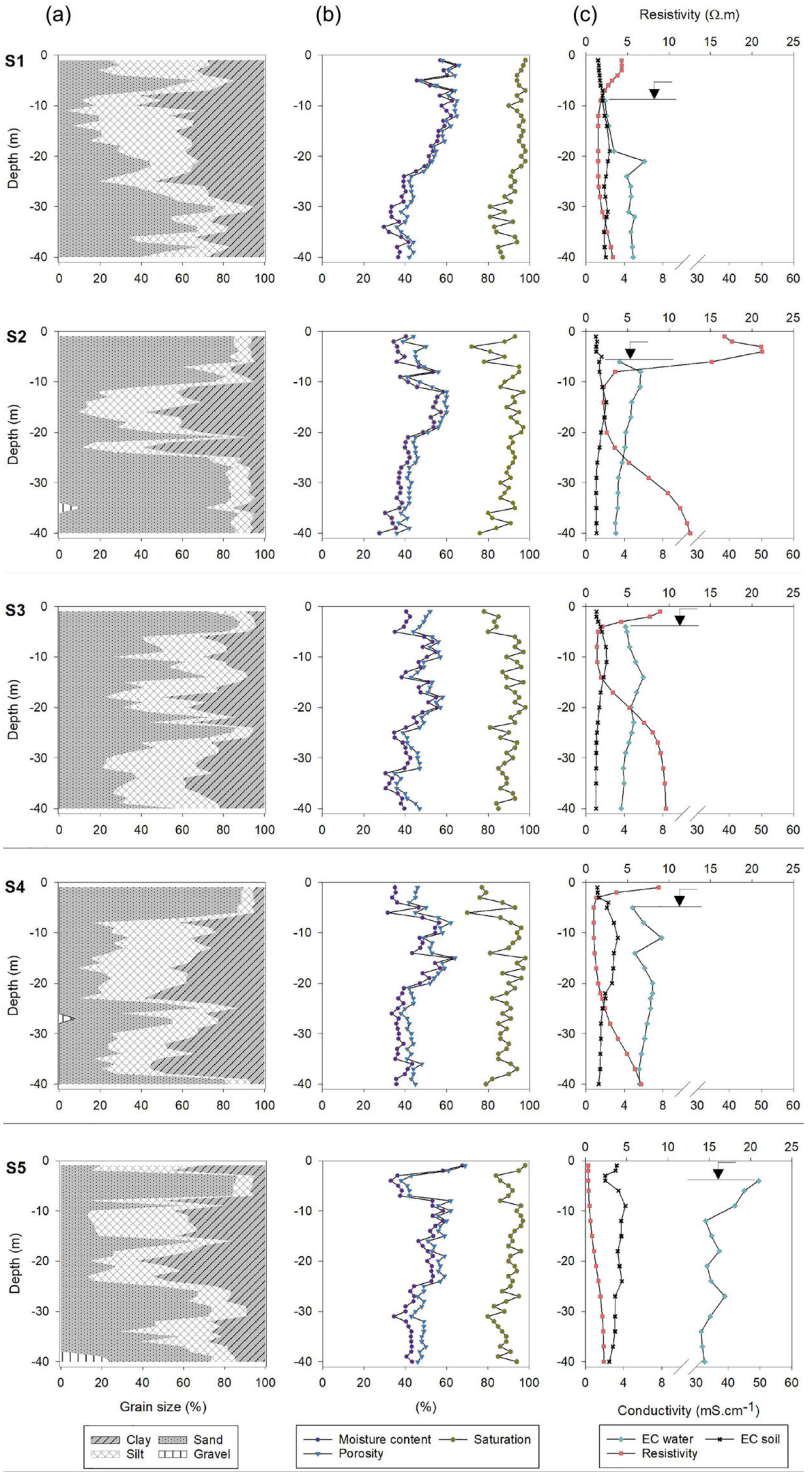


**FIGURE 5** Soil properties obtained from cores at 1 m depth intervals at site S1–S4. Part (a) represents soil texture. (b) Moisture content, porosity and degree of saturation in the soil pores. (c) Electrical conductivity (EC) of soil and water and resistivity of soil extracted from electrical resistivity tomography (ERT) profiles at borehole positions. In (c) *x*-axes (conductivity axis) breaks were applied from EC 10 to 30 mS cm$^{-1}$ due to the high EC of water at site S5. Arrows illustrate the water tables.

## Principal component analysis

PCA was used to identify saline water tables and their depth based on the soil and water properties at case study sites S1–S4. Site S5 has not been included in the PCA due to its proximity to the sea and different land-use (Figure 6).

The PCA is a multivariate statistical method that reduces the dimensionality of large data sets. The number of principal components (PCs) corresponds to the number of variables used in the PCA analysis (Greenacre et al., 2022). In this section, seven variables were used for PCA analysis, including clay, sand, bulk density, moisture content, resistivity and EC of soil and water samples.

Two PCs (PC1 and PC2) explain 74.1% of the variance in the data set (Table 2). PC3 potentially explains additional 15%; however, PC3 was mainly linked to

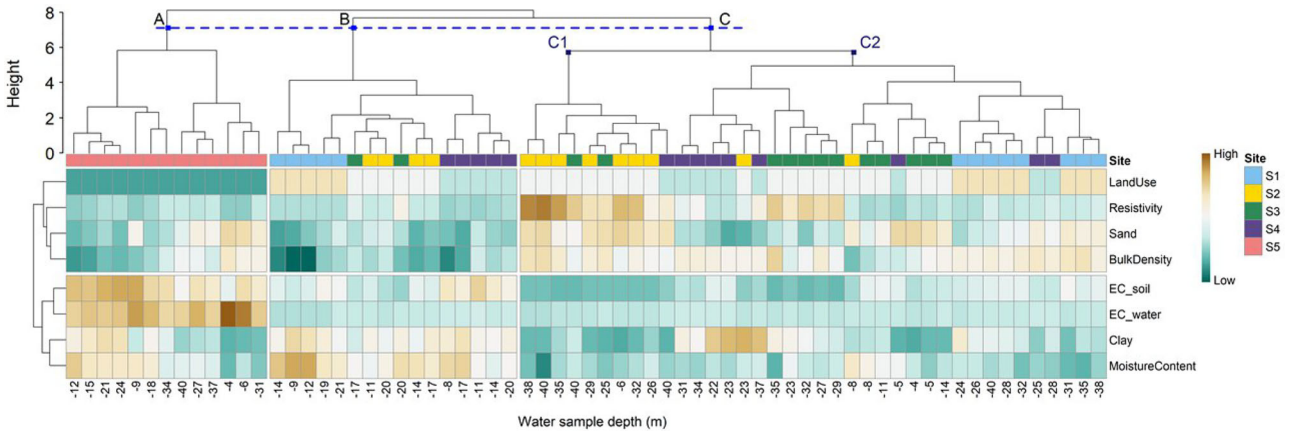


**FIGURE 6** Heat map for soil properties and soil salinity at different sample depths at the five study sites. The heat map illustrates a hierarchical analysis with two dendrograms. The top dendrogram shows clusters based on sample depths, whereas the left dendrogram groups variables that have similar properties. Land-use is indicated as dark petrol for shrimp farming, light petrol for single rice cropping, white for double rice cropping and yellow for triple rice cropping. All other variables are shown on a standardized colour scale from low (dark petrol) to high (dark brown) by subtracting column means from columns and divide it by column standard deviations.

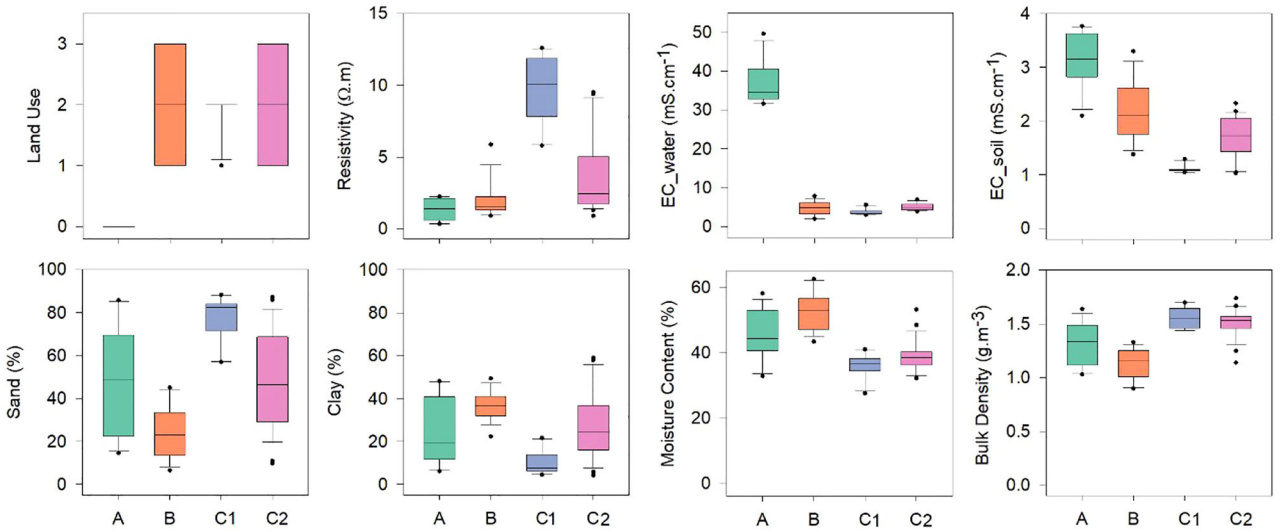


**FIGURE 7** Representation of electrical resistivity and related variables in three main groups derived from the heat map in Figure 6 as boxplots. Group C is divided into two sub-groups: C1 and C2. For land-use, 0 = shrimp farming, 1 = single rice cropping, 2 = double rice cropping, 3 = triple rice cropping.

**TABLE 2** Contribution of seven principal components (PCs) to variance in the data set.

| | PC1 | PC2 | PC3 | PC4 | PC5 | PC6 | PC7 |
|---|---|---|---|---|---|---|---|
| Standard deviation | 1.920 | 1.222 | 1.052 | 0.639 | 0.445 | 0.261 | 0.177 |
| Proportion of variance | 0.527 | 0.214 | 0.158 | 0.058 | 0.028 | 0.010 | 0.005 |
| Cumulative proportion | 0.527 | 0.741 | 0.899 | 0.957 | 0.986 | 0.996 | 1 |

soil properties (data not shown), which are already sufficiently covered by the first two PC which clearly distinguish between clay and sandy soils.

In Figure 8, PC1 distinguishes groups B and C as clustered in Figure 6, whereas PC2 comprises two groups associated with water quality: saline water and non-saline water.

In the non-saline group, samples with high resistivity values combined with low EC values form a distinct cluster. This high resistivity cluster (>5.8 Ω m at S2 and >7.5 Ω m at S3) represents deeper soil layers in S2 (26–40 m) and in S3 (23–40 m). Samples in the top layer in S2 (6 m) and in S3 (4–5 m) also appear in this group. The elevated resistivity in this cluster is related to high sand content and low moisture content. In addition to the high resistivity cluster, samples from 9 m to 19 m of site S1 appear in the non-saline group with low resistivity (<1.6 Ω m) due to their high clay and moisture content.

Within the saline group, samples from shallow depths group in between the bi-plots of clay content and EC

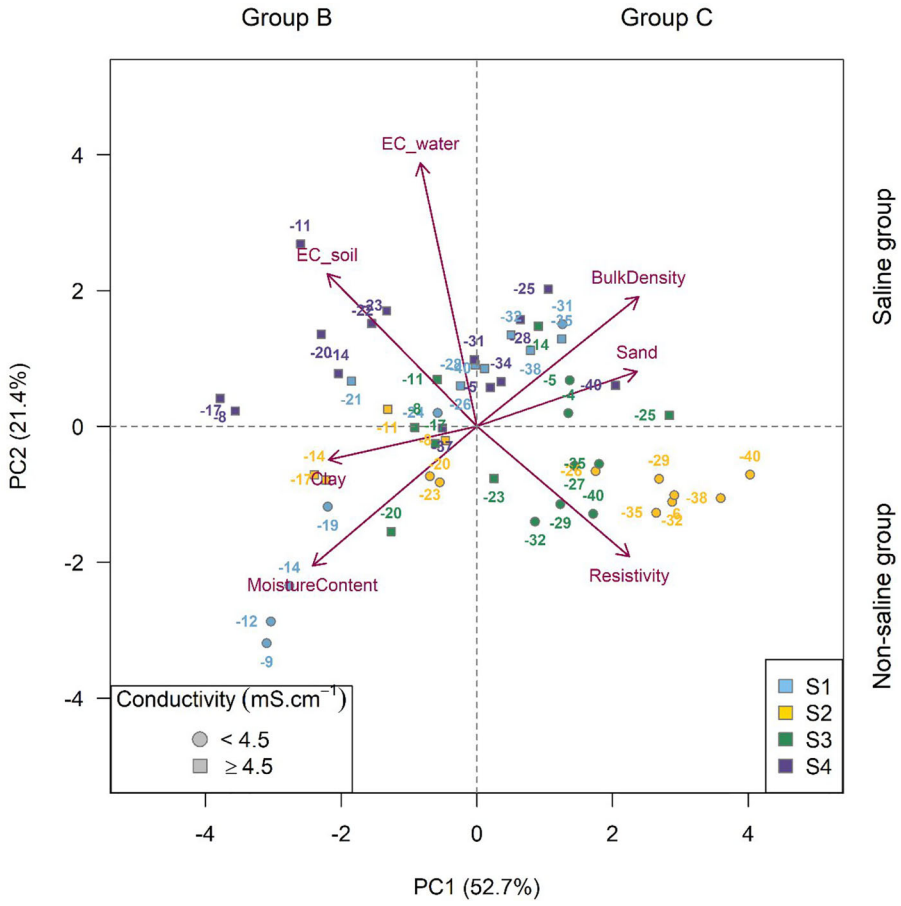


**FIGURE 8** Principle component analysis for two principle components: PC1 and PC2 at four sites, S1–S4. The numbers indicate the depth in meters at which the water samples were taken.

of soil, whereas samples of the medium depths cluster between the bi-plots of EC of soil and the bulk density. The cluster with medium depths comprises most samples of site S1 (26–40 m), S3 (11–14 m) and S4 (22–34 m). Resistivity values in this cluster vary from 1.6 Ω m to 3.3 Ω m, 1.4 Ω m to 2.1 Ω m and 1.8 Ω m to 5.3 Ω m for site S1, S3 and S4, respectively. Only the sample of site S4 at a shallow depth (5 m) appears in this cluster with a resistivity of 0.9 Ω m. However, most of the shallow samples at the remaining sites, including S1 (21 m), S2 (8 m) and S3 (8 m), are located between clay and EC of soil with resistivity of less than 2.5 Ω m. Low resistivity in the middle depths is mainly affected by salinity, whereas in the shallow depths, it is also influenced by soil properties, such as clay and moisture content.

The results from the PCA demonstrate that resistivity below 3 Ω m represents the threshold where the saline water table begins. The saline groundwater table decreases towards inland, from 5 m at S4 to 20 m at S1, whereas the thickness of saline water table decreases from 23 m at S4 to 3 m at site S2.

With respect to the saline water level, the results from PCA are consistent with ERT profiles at most of case study sites, S2–S4 (Figure 2). At site S1, the interface between freshwater and saline water is unclear in the ERT profile due to the uniformity in resistivity (<2 Ω m) from around 10 m to 40 m depth.

## CONCLUSIONS

The aim of this study was to evaluate the suitability of the ERT as a geophysical method for identifying saline groundwater tables that may pose a threat to rice production systems in the VMD due to capillary rise. The geophysical data from ARESII were supplemented with data from 40 m borehole cores to test the interpretability and thus the reliability of data from ERT. Combining the ARES II and the borehole data with the cluster and PCA analysis allowed identifying location and thickness of the shallow water table as well as the boundary between freshwater and saltwater layers at locations with highly variable resistivity. Resistivity values smaller than 3 Ω m were identified as indicative for saline water. Thus, we were able to show that the shallow groundwater below rice fields in the case study sites in Tra Vinh province

consists of saline water, with the thickness of the saline water layer increasing towards the sea. Only at sites that yield nearly homogenous resistivity values, the interpretation of ARES II data may require additional drilling or geological reference data, such as soil type.

We found no clear link between the shallow saline water table and rice cropping patterns in Tra Vinh province, indicating no capillary rise between the shallow water table and the top soil; however, this may change with increasing sea level rise. Overall, ARES II showed great potential to detect and monitor eventual changes in extent and salinity of near surface water layers.

We have used ERT for the first time in the VMD, with the aim to detect and characterize salinity beneath rice fields. With the results, we have provided evidence that ERT is a powerful tool for characterizing and monitoring salt intrusion into the shallow water layer in the VMD and other rice-growing areas in river deltas around the world, which are prone to saltwater intrusion due to climate change induced sea level rise.

## ACKNOWLEDGEMENTS

This work has been funded by the Federal Ministry of Education and Research (BMBF, Germany) in the project RiSaWa (project number 031B0724).

Open access funding enabled and organized by Projekt DEAL.

## DATA AVAILABILITY STATEMENT

The data that support the findings of this study are available upon reasonable request from the corresponding author.

## REFERENCES

Araya Vargas, J., Gil, P.M., Meza, F.J., Yáñez, G., Menanno, G., García-Gutiérrez, V. et al. (2021) Soil electrical resistivity monitoring as a practical tool for evaluating irrigation systems efficiency at the orchard scale: a case study in a vineyard in Central Chile. *Irrigation Science*, 39, 123–143. https://doi.org/10.1007/s00271-020-00708-w

Brouwer, C., Goffeau, A. & Heibloem, M. (1985) *Irrigation water management: training manual no. 1 – introduction to irrigation*. Rome: FAO. https://www.fao.org/3/r4082e/r4082e08.htm#7.2%20salinity [Assessed 20 October 2022]

CGIAR Research Program on Climate Change, Agriculture and Food Security - Southeast Asia (CCAFS SEA). (2016) *Assessment report: the drought and salinity intrusion in the Mekong River Delta of Vietnam*. Hanoi, Vietnam: CGIAR Research Program on Climate Change, Agriculture and Food Security (CCAFS).

Cimpoiaşu, M.O., Kuras, O., Pridmore, T. & Mooney, S.J. (2020) Potential of geoelectrical methods to monitor root zone processes and structure: a review. *Geoderma*, 365, 114232. https://doi.org/10.1016/j.geoderma.2020.114232

Cong-Thi, D., Dieu, L.P., Thibaut, R., Paepen, M., Ho, H.H., Nguyen, F. et al. (2021) Imaging the structure and the saltwater intrusion extent of the Luy river coastal aquifer (Binh Thuan, Vietnam) using electrical resistivity tomography. *Water (Switzerland)*, 13, 1743. https://doi.org/10.3390/w13131743

de Franco, R., Biella, G., Tosi, L., Teatini, P., Lozej, A., Chiozzotto, B. et al. (2009) Monitoring the saltwater intrusion by time lapse electrical resistivity tomography: the Chioggia test site (Venice Lagoon, Italy). *Journal of Applied Geophysics*, 69, 117–130. https://doi.org/10.1016/j.jappgeo.2009.08.004

El-Hamdouchi, A. & Willett, P. (1989) Comparison of hierarchic agglomerative clustering methods for document retrieval. *The Computer Journal*, 32, 220–227. https://doi.org/10.1093/comjnl/32.3.220

FAO. (2016) *"El NiÑo" event in Viet Nam – Agriculture, food security and livelihood needs assessment in response to drought and salt water intrusion*. https://www.fao.org/3/i6020e/i6020e.pdf

Galazoulas, E.C., Mertzanides, Y.C., Petalas, C.P. & Kargiotis, E.K. (2015) Large scale electrical resistivity tomography survey correlated to hydrogeological data for mapping groundwater salinization: a case study from a multilayered coastal aquifer in Rhodope, Northeastern Greece. *Environmental Processes*, 2, 19–35. https://doi.org/10.1007/s40710-015-0061-y

Gemail, K., Samir, A., Oelsner, C., Mousa, S.E. & Ibrahim, S. (2004) Study of saltwater intrusion using 1D, 2D and 3D resistivity surveys in the coastal depressions at the eastern part of Matruh area, Egypt. *Near Surface Geophysics*, 2, 103–109. https://doi.org/10.3997/1873-0604.2004007

Giao, P.H., Chung, S.G., Kim, D.Y. & Tanaka, H. (2003) Electric imaging and laboratory resistivity testing for geotechnical investigation of Pusan clay deposits. *Journal of Applied Geophysics*, 52, 157–175. https://doi.org/10.1016/S0926-9851(03)00002-8

Gołębiowski, T. & Jarosińska, E. (2019) Application of GPR and ERT methods for recognizing of gypsum deposits in urban areas. *Acta Geophysica*, 67, 2015–2030.

Greenacre, M., Groenen, P.J.F., Hastie, T., D'Enza, A.I., Markos, A. & Tuzhilina, E. (2022) Principal component analysis. *Nature Reviews Methods Primers*, 2, 100. https://doi.org/10.1038/s43586-022-00184-w

Ha, Q.K., Tran Ngoc, T.D., Le Vo, P., Nguyen, H.Q. & Dang, D.H. (2022) Groundwater in Southern Vietnam: understanding geochemical processes to better preserve the critical water resource. *Science of the Total Environment*, 807(part 2), 151345. https://doi.org/10.1016/j.scitotenv.2021.151345

Kolde, R. (2019) *pheatmap: pretty heatmaps*. R package version 1.0.12. https://CRAN.R-project.org/package=pheatmap

Loke, M.H. (2021) *Tutorial: 2-D and 3-D electrical imaging surveys*. https://www.researchgate.net/publication/264739285_Tutorial_2-D_and_3-D_Electrical_Imaging_Surveys [Accessed 17 August 2022]

Minderhoud, P.S.J., Coumou, L., Erkens, G., Middelkoop, H. & Stouthamer, E. (2019) Mekong delta much lower than previously assumed in sea-level rise impact assessments. *Nature Communications*, 10, 3847. https://doi.org/10.1038/s41467-019-11602-1

Mohamaden, M. & Ehab, D. (2017) Application of electrical resistivity for groundwater exploration in Wadi Rahaba, Shalateen, Egypt. *NRIAG Journal of Astronomy and Geophysics*, 6, 201–209. https://doi.org/10.1016/j.nrjag.2017.01.001

Murtagh, F. & Contreras, P. (2012) Algorithms for hierarchical clustering: an overview. *Wiley Interdisciplinary Reviews: Data Mining and Knowledge Discovery*, 2, 86–97. https://doi.org/10.1002/widm.53

Nguyen, L.D., Nguyen, T.V.K., Nguyen, D.V., Tran, A.T., Nguyen, H.T., Heidbüchel, I. et al. (2021) Groundwater dynamics in the Vietnamese Mekong Delta: trends, memory effects, and response times. *Journal of Hydrology: Regional Studies*, 33, 100746. https://doi.org/10.1016/j.ejrh.2020.100746

Nowroozi, A.A., Horrocks, S.B. & Henderson, P. (1999) Saltwater intrusion into the freshwater aquifer in the eastern shore of Virginia: a reconnaissance electrical resistivity survey. *Journal of Applied Geophysics*, 42, 1–22. https://doi.org/10.1016/S0926-9851(99)00004-X

Palacky, G.J. (1987) Resistivity characteristics of geologic targets. *Electromagnetic Methods in Applied Geophysics*, 1, 53–129. https://doi.org/10.1190/1.9781560802631.ch3

R Core Team. (2021) *R: a language and environment for statistical computing*. Vienna, Austria: R Foundation for Statistical Computing. https://www.R-project.org/

Rao, S., Lesparre, N., Flores-Orozco, A., Wagner, F., Kemna, A. & Javaux, M. (2020) Imaging plant responses to water deficit using electrical resistivity tomography. *Plant and Soil*, 454, 261–281. https://doi.org/10.1007/s11104-020-04653-7

Riwayat, A.I., Ahmad Nazri, M.A. & Zainal Abidin, M.H. (2018) Application of electrical resistivity method (ERM) in groundwater exploration. *Journal of Physics: Conference Series*, 995, 012094. https://doi.org/10.1088/1742-6596/995/1/012094

Samouëlian, A., Cousin, I., Tabbagh, A., Bruand, A. & Richard, G. (2005) Electrical resistivity survey in soil science: a review. *Soil and Tillage Research*, 83, 173–193. https://doi.org/10.1016/j.still.2004.10.004

Schneider, P. & Asch, F. (2020) Rice production and food security in Asian Mega deltas – a review on characteristics, vulnerabilities and agricultural adaptation options to cope with climate change. *Journal of Agronomy and Crop Science*, 206, 491–503. https://doi.org/10.1111/jac.12415

Shevnin, V., Delgado Rodríguez, O., Mousatov, A., Flores Hernández, D., Zegarra Martínez, H. & Ryjov, A. (2006) Estimation of soil petrophysical parameters from resistivity data: application to oil-contaminated site characterization. *International Geophysics*, 45, 179–193.

Takahashi, A., Hashimoto, M., Hu, J., Takeuschi, K. & Tsai, M. (2019) Hierarchical cluster analysis of dense GPS data and examination of the nature of the clusters associated with regional tectonics in Taiwan. *Geophysical Research Letters: Solid Earth*, 124, 5174–5191. https://doi.org/10.1029/2018JB016995

Tan, X., Shao, D. & Liu, H. (2014) Simulating soil water regime in lowland paddy fields under different water managements using HYDRUS-1D. *Agricultural Water Management*, 132, 69–78. https://doi.org/10.1016/j.agwat.2013.10.009

Tran, D.A., Tsujimura, M., Pham, H.V., Nguyen, T.V., Ho, L.H., Le Vo, P. et al. (2022) Intensified salinity intrusion in coastal aquifers due to groundwater over extraction: a case study in the Mekong Delta, Vietnam. *Environmental Science and Pollution Research*, 29, 8996–9010. https://doi.org/10.1007/s11356-021-16282-3

Tran, P.H. (2020) Assessment of changes in the structure land use in Tra Vinh Province under the scenarios of climate change and sea level rise. *Vietnam Journal of Science and Technology*, 58, 70–83. https://doi.org/10.15625/2525-2518/58/1/13982

Tyler, R.H., Boyer, T.P., Minami, T., Zweng, M.M. & Reagan, J.R. (2017) Electrical conductivity of the global ocean. *Earth, Planets and Space*, 69, 1–10. https://doi.org/10.1186/s40623-017-0739-7

Van Kien, N., Hoang Han, N. & Cramb, R. (2020) Trends in rice-based farming systems in the Mekong Delta. In: Cramb, R. (Ed.) *White gold: the commercialisation of rice farming in the lower Mekong Basin*. Singapore: Palgrave Macmillan. https://doi.org/10.1007/978-981-15-0998-8_17

Yen, B.T., Son, N.H., Tung, L.T., Amjath-Babu, T.S. & Sebastian, L. (2019) Development of a participatory approach for mapping climate risks and adaptive interventions (CS-MAP) in Vietnam's Mekong River Delta. *Climate Risk Management*, 24, 59–70. https://doi.org/10.1016/j.crm.2019.04.004

Zohdy, A.A.R., Martin, P.M. & Bisdorf, R.J. (1993) *A study of seawater intrusion using direct-current soundings in the southeastern part of the Oxnard Plain, California*, vol. 93. US Geological Survey. https://doi.org/10.3133/ofr93524

**How to cite this article:** Nguyen, V.H., Germer, J., Duong, V.N., Asch, F. (2023) Soil resistivity measurements to evaluate subsoil salinity in rice production systems in the Vietnam Mekong Delta. *Near Surface Geophysics*, 21, 288–299. https://doi.org/10.1002/nsg.12260